Numerical Simulation of the Drill String Buckling Behavior in Horizontal Wells Considering the Orthotropic Friction

Jianxun LIU*, Hualin ZHENG**, Yuchun KUANG***, Xiaofeng XU****, Yonghui LIU*****

*Southwest Petroleum University, Chengdu, 610500, China, E-mail: swpuliujiianxun@126.com
**Southwest Petroleum University, Chengdu, 610500, China, E-mail: zhl@swpu.edu.cn
***Southwest Petroleum University, Chengdu, 610500, China, E-mail: swpikyc@126.com
****PetroChina Jidong Oilfield Company, Tangshan, China, E-mail: xxf@petrochina.com.cn
*****PetroChina Jidong Oilfield Company, Tangshan, China, E-mail: jd_liuyh@petrochina.com.cn

1. Introduction

Buckling is an important issue in oil and gas industry [1]. The drill string can buckle into a sinusoidal or helical buckling configuration under the co-action of the gravity, bending moment, contact force as well as friction between the drill string and borehole. Buckling not only leads to the increase of contact force and friction, also impacts the axial force transfer and exerts the difficulty of well trajectory control. Therefore, the study of the drill string buckling behavior is highly significant in engineering.

According to whether the consideration of friction or not, up to date, the buckling research can be classified in two categories: the conservative and the non-conservative system. Although the great achievements of the conservative system are beneficial to better understand the buckling behaviour [2–4], the accuracy of the predicted formulations needs to be further discussed for the absence of friction [5]. In the context of the non-conservative system, in 2006, Gao Deli [5] obtained expressions for the sinusoidal and helical bucking force when the axial and tangential friction was considered. Later, Gao and Miska [6,7] considered the effect of the tangential friction, and induced the formulations for the sinusoidal and helical buckling force. Recently, Hajianmaleki and Daily [8] studied the critical buckling and the axial force transfer issue using the finite element model established in Abaqus. Miller et al. [9], based on the finite element method, researched the buckling behavior of the Kirchhoff rod constrained in a horizontal pipe under the influence of the isotropic friction. However, the current studies on the non-conservative system, though considering the friction between the drill string and the borehole, usually simplify it as the unidirectional or the isotropic friction, which is quite distinct from the actual condition.

Actually, in the actual operation the switch between the sliding and the rotary drilling mode may result in the spiral borehole and the tortuosity, which further leads to the difference between the axial and the tangential morphology [10–13]. The difference in morphology, however, inevitably contributes to the difference of the axial and the tangential friction coefficient [14,15]. If we still take the unidirectional or the isotropic friction assumption, there may cause a big error. So, it is quite necessary to analyse the drill string buckling behavior under the influence of the orthotropic friction.

In this paper, we regard the friction between the drill string and the borehole as the orthotropic friction, and establish a FE model for the horizontal drill string and the borehole system based on the finite element method. Then, we examine the effect of the orthotropic friction on the buckling behavior of the drill string in sliding mode. The conclusions can complement the existing theoretical models and provide guidance for field operations.

2. FE model of the horizontal drill string

2.1. Assumptions

The following assumptions are employed in the modeling process:

1. The drill string is treated as an assembly of elastic pipes with homogeneous properties;

2. The axis of the borehole is straight with a circular section;

3. The drill string continuously contacts with the borehole, and the influence of the torque, threaded connections and local notches is ignored;

4. The friction coefficient reflects the mechanical friction between the drill string and borehole, the sediment and the tortuosity [11];

5. The effect of temperature on material properties is ignored;

6. The effect of drill fluid flow is neglected.

2.2. FE model of the drill string

As shown in Fig. 1, the drill string lies on the low side of the borehole, and might buckle into a sinusoidal or helical buckling configuration with the increase of the compression on the top end (the left end in Fig. 1). We discretize the drill string into beam elements along the axial direction, according to the Euler-Bernoulli beam theory. Each element has two nodes, 6 degrees of freedom at each node. The beam element can simulate the action of the tension-compress-torque-bending moment. A global and local coordinate are established at the left end of the borehole and the center of the beam element section to describe the actual configuration and the internal deformation of the drill string, respectively.

As shown in Fig. 1, b and Fig. 1, c, the node force and displacement vector can be expressed by the Eq. (1) and Eq. (2) in the local coordinate system:

$$\{u_e\} = \left\{ u_i\, v_i\, w_i\, \theta_{xi}\, \theta_{yi}\, \theta_{zi}\, u_j\, v_j\, w_j\, \theta_{xj}\, \theta_{yj}\, \theta_{zj} \right\}^T, \quad (1)$$

$$\{F_e\} = \left\{R_{xi}\,R_{yi}\,R_{zi}\,M_{xi}\,M_{yi}\,M_{zi}\,R_{xj}\,R_{yj}\,R_{zj}\,M_{xj}\,M_{yj}\,M_{zj}\right\}^T, \quad (2)$$

where: u, v, w and R_x, R_y, R_z represent the line displacement and the node force in x-,y-, and z-direction, respectively; θ_x, θ_y, θ_z and M_x, M_y, M_z characterizes the angular displacement and the moment in x-,y-, and z-direction, respectively; the subscript "i" and "j" of each displacement and force represent the component of each node.

a

b   c

Fig. 1 a-Mechanical model of the drill string and borehole system; b- nodal displacement of a beam element; c- force vector of a beam element

The kinetic energy of the beam element can be defined as:

$$T_e = \frac{1}{2}\int_{V_0}\rho\{\dot{u}_e\}^T\{\dot{u}_e\}dV = \frac{1}{2}\{\dot{u}_e\}^T\{m_e\}\{\dot{u}_e\}, \quad (3)$$

where: ρ is the material density, $\{m_e\}$ is the element mass matrix.

The potential energy of the beam element can be expressed as:

$$U_e = \frac{1}{2}\int_{V_0}\{\varepsilon\}^T\{\sigma\}dV - \int_{A_e}\{u_e\}^T\{F_A\}dA -$$
$$-\int_{V_e}\{u_e\}^T\{F_V\}dV - \{u_e\}^T\{F_e\}, \quad (4)$$

where: $\{F_e\}, \{F_V\}, \{F_A\}$ are the node force, the unit force and the unit surface force, respectively.

Substituting Eq. (3) and Eq. (4) into the Lagrangian equation, then the kinetic control equation of the beam element in the local coordinate system is obtained [16]:

$$\{m_e\}\{\ddot{u}_e\} + \{C_e\}\{\dot{u}_e\} + \{K_e\}\{u_e\} = \{F_e\}, \quad (5)$$

where: $\{C_e\}$ and $\{K_e\}$ are the damping matrix and the stiffness matrix, respectively.

After the coordinate transformation, the motion control equation of the entire drill string can be induced in the global coordinate system [17]:

$$[M]\{\ddot{U}\} + [C]\{\dot{U}\} + [K]\{U\} = \{F\}, \quad (6)$$

where: $\{\ddot{U}\}, \{\dot{U}\}, \{U\}, \{F\}$ are the acceleration matrix, the velocity matrix, the displacement matrix and the external matrix, respectively; $[M], [C], [K]$ are the mass matrix, the damping matrix and the stiffness matrix.

2.3. Contact and friction between the drill string and the borehole

In the sliding process, the drill string may deform laterally or helically due to the effect of factors such as gravity, compression and irregular bottom, then might contact with the borehole at some certain points. Once the contact occurs, as shown in Fig. 2, it will impact the friction between the drill string and the borehole.

A finite element method based on the 3D cylinder-to-cylinder line contact pair is employed to characterize the contact between the drill string and the borehole. By defining the gap function g_n, it is checked whether or not the contact occurs:

$$g_n = (R - r_p) - d = \begin{cases} > 0 & \text{if no contact,} \\ \leq 0 & \text{if contact,} \end{cases} \quad (7)$$

where: d is the minimum distance between the drill string and the borehole, determined by inspecting the relative position of the check points i or j to the line segment P_iP_j, R is the inside diameter of the borehole, r_p is the outside diameter of the drill string.

When $g_n \leq 0$, the contact force between the drill string and the borehole is calculated according to the Hertzian contact theory, then assembled into the external force matrix $\{F\}$:

$$N = kg_n, \quad (8)$$
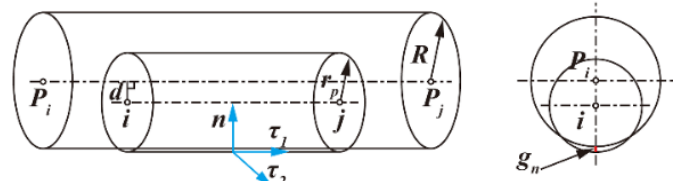
where: k is the contact stiffness.

Fig. 2 Schematic of the contact model between the drill string and the borehole

Once the contact is declared, the friction and the induced friction torque are computed according to the orthotropic friction:

$$f = N\sqrt{\mu_{\tau1}^2\cos^2\theta + \mu_{\tau1}^2\sin^2\theta}, \quad (9)$$
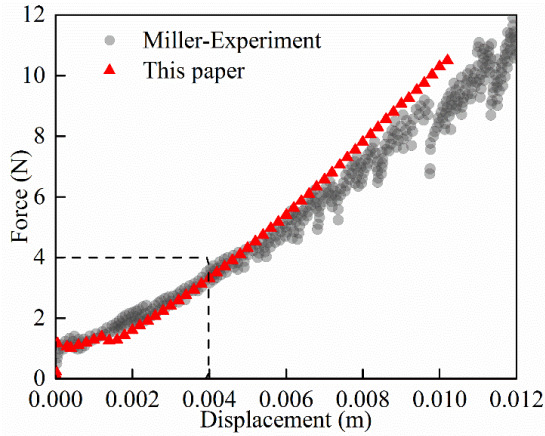
$$T_f = fr_p, \quad (10)$$

where: $\mu_{\tau1}$ and $\mu_{\tau2}$ are the friction coefficient along the axial and tangential direction, θ is the angle between the axial displacement and the tangential direction. Note that when $\mu_{\tau1} = \mu_{\tau2}$, there is the case of the isotropic friction.
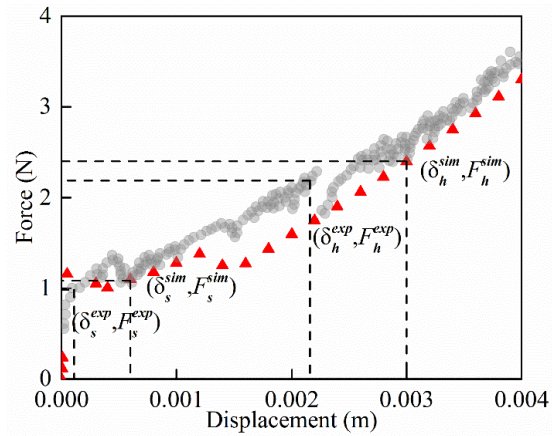
2.4. Boundary condition

In the simulation, the translational freedoms U_y and U_z of the loaded end (the left end) of the drill string are restrained while other freedoms are free, which means the drill string can move freely along the axial direction of the borehole. The right end of the drill string is pinned, which indicates that the translational freedoms are fixed. In this study, the simulation is undertaken in three stages. Firstly, the gravity is applied in 10seconds. Secondly, a small transverse force $P=0.02 \times mg\ sin(0.5\pi t)$ is loaded in the middle of the drill string in another 10 seconds, acting as a trigger for the onset of the buckling [8]. Finally, the drill string is compressed along the x-direction with a steady speed of 0.2 mm/s until the fully helical buckling occurs. Based on the implicit algorithm, the Newton-Raphson method is employed to solve the Eq. (6).

2.5. Verification

Miller et al. [9] conducted an experimental investi-gation on the buckling behavior of a Nitinol rod compressed axially inside an acrylic pipe. The inner diameter of the acrylic pipe is 19 mm, the outer diameter of the rod is 16 mm, and the length is 3.095 m. The elastic modulus is 68 GPa, the Poisson's ratio is 0.3, the density is 6538 kg/m^3, and the friction coefficient is 0.3. We utilize the experiment of Miller et al. [9] to validate the accuracy of the FEA model established in this paper.

For comparison, the force-displacement curve of the top end is selected to characterize the critical buckling forces [8]. As seen in Fig. 4, a, the numerical result agrees well with that of the experiment. Further, as shown in Fig. 4, b, the sinusoidal buckling force and the helical buckling force in the simulation are 1.05 N and 2.39 N, respectively. While the critical buckling forces in the experiment are 0.98 N and 2.18 N. The errors are respectively 7.14% and 9.63%, within the scope of the project. The comparison with the experiment demonstrates that the FEA model has a high accuracy for predicting the critical buckling forces.

Fig. 3 a - Comparion of the force-displacement curve between the simulation and the experiment; b - Zoom of the region inside the dashed box in Fig. 3, a

3. Results and discussion

In order to examine the influence of the orthotropic friction on the buckling behavior of the horizontal drill string, we conduct the simulation in two cases (Case1: $\mu_{\tau1}$ varies from 0.1 to 0.4 and $\mu_{\tau2}$=0.3; Case 2: $\mu_{\tau1}$=0.3 and $\mu_{\tau2}$ varies from 0.1 to 0.4), respectively. The basic parameters of the drill string and the borehole system are shown in Table 1.

Table 1

Basic parameters of the drill string and borehole system

Parameter	Value
Inner diameter(ID) of the borehoele /mm	216
Outer diameter(OD) of the drill string/mm	127
Inner diameter(ID) of the drill string/mm	108
Length of the drill string/m	200
Elastic modulus/GPa	210
Poisson's ratio	0.3
Density of the drill string /(kg·m³)	7850
Inner diameter(ID) of the borehoele /mm	216

3.1. Effect of the orthotropic friction on critical buckling forces

Table 2 and Fig. 4 quantitatively demonstrate the critical buckling forces in each case. Interestingly, Fig. 4 shows that in Case 1, as the axial friction coefficient increases, the sinusoidal buckling force decreases and the helical buckling force increases. This indicates that only considering the tangential friction may overestimate the sinusoidal buckling force and underestimate the helical buckling force. While in Case 2, as the tangential friction coefficient increases, the helical buckling force decreases, which means only considering the axial friction may underestimate the helical buckling force. This phenomenon, to our best knowledge, is quite different from the results of the literature [5–7], and has not been reported before.
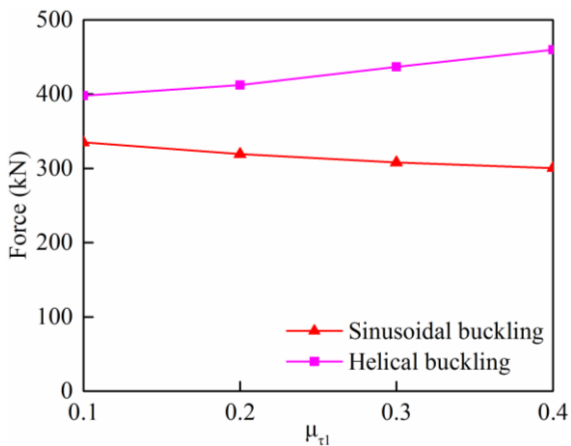
Fig. 4 also highlights the difference of the buckling resistance capacity of the drill string under the effect of the isotropic and orthotropic friction. For instance, when $\mu_{\tau1}$=0.1, $\mu_{\tau2}$=0.3, the sinusoidal buckling force is 334.59 kN, which is about 8.28% larger than the corresponding value when $\mu_{\tau1}$= $\mu_{\tau2}$=0.3. While $\mu_{\tau1}$=0.3 and $\mu_{\tau2}$=0.1, the sinusoidal

buckling force is 217.26 kN, which is about 29.44% less than the corresponding value when $\mu_{\tau 1}=\mu_{\tau 2}=0.3$.
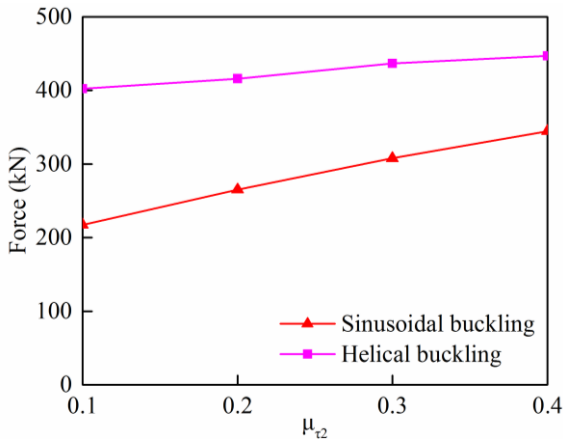
Table 2

Effect of the orthotropic friction on critical buckling forces

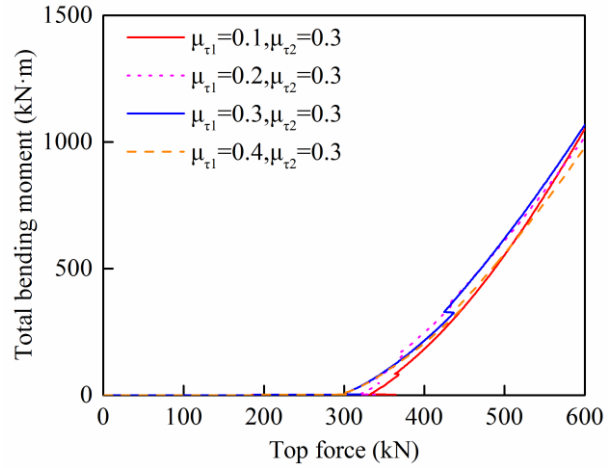| Friction coefficient		Sinusoidal buckling force, kN	Helical buckling force, kN
$\mu_{\tau 1}$ (with $\mu_{\tau 2}=0.3$)	0.1	334.59	397.98
	0.2	319.01	412.23
	0.3	307.91	436.54
	0.4	300.26	459.84
$\mu_{\tau 2}$ (with $\mu_{\tau 1}=0.3$)	0.1	217.26	402.02
	0.2	265.19	416.08
	0.3	307.91	436.54
	0.4	344.51	447.02

Fig. 4 Effect of the orthotropic friction on critical buckling forces: a - Case 1; b - Case 2

In one word, neither the hypothesis of the unidirectional friction or the isotropic friction can precisely calculate the critical buckling forces. The effect of the orthotropic friction should be fully taken into account in order to accurately predict the buckling resistance capacity.
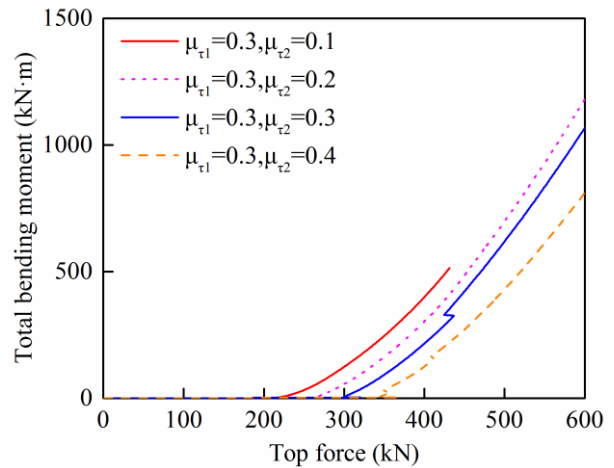
3.2. Effect of the orthotropic friction coefficient on bending moment

Buckling can exert the bending stress of the drill string, and increase the risk of fatigue [5]. The total bending

moment reflects the deformation of the drill string. Results, quantitatively indicated in Fig. 5, exhibit the relationship between the bending moment and the top force in each case. The increase of the top force considerably escalates the deformation of the drill string. The greater the axial friction coefficient, as well as the smaller the tangential friction coefficient, the earlier the sinusoidal buckling occurs. This demonstrates that the influence of the tangential friction on the bending moment of the drill string is greater than that of the axial friction.

Fig. 5 Effect of the orthotropic friction on bending moment: a – Case 1; b – Case 2

3.3. Effect of the orthotropic friction on each frictional force

The total friction force f between the drill string and the borehole includes the axial friction force $f_{\tau 1}$ and the tangential friction force $f_{\tau 2}$, which are respectively computed by:

$$f_{\tau_1} = \mu_{\tau 1} N, \ f_{\tau_2} = \mu_{\tau 2} N. \tag{11}$$

The axial friction force ratio $\lambda_{\tau 1}$ and the tangential friction force ratio $\lambda_{\tau 2}$ are defined as:

$$\left.\begin{array}{l} \lambda_{\tau 1} = \dfrac{f_{\tau 1}}{f} \times 100\% = \dfrac{f_{\tau 1}}{\sqrt{f_{\tau 1}^2 + f_{\tau 2}^2}} \times 100\%, \\[4mm] \lambda_{\tau 2} = \dfrac{f_{\tau 2}}{f} \times 100\% = \dfrac{f_{\tau 2}}{\sqrt{f_{\tau 1}^2 + f_{\tau 2}^2}} \times 100\%, \end{array}\right\}. \quad (12)$$

Results, quantitatively indicated in Figs. 6 – 9, feature the evolution of the friction forces and their ratios in two cases. In the stable stage, $\lambda_{\tau 1} \approx 100\%$ (Fig. 8), which presents $f \approx f_{\tau 1}$ (Fig. 6). When the sinusoidal bucking occurs, $f_{\tau 1}$ decreases and $f_{\tau 2}$ increases instantaneously (Fig. 6). At

this moment, $\lambda_{\tau 2}$ reaches the maximum, which means $\lambda_{\tau 1}$ reaches the minimum. After that, when the axial displacement increases, the increase of $f_{\tau 1}$ is greater than $f_{\tau 2}$, resulting in the decrease of $\lambda_{\tau 2}$ and the increase of $\lambda_{\tau 1}$.

Figs. 8 and 9 also reveal that the increase of the friction coefficient in any direction may trigger the increase of the corresponding ratio, and the decrease of the another ratio. Notably, in Fig. 8, c and d and Fig. 9, a and b, when the critical buckling occurs, $\mu_{\tau 1}/\mu_{\tau 2} > 1$ and $\mu_{\tau 2} \leqslant 50\%$. This implies that the hypothesis that $\mu_{\tau 1}=0$, $\mu_{\tau 2} \approx \mu$ proposed in the literature [6, 7] is only valid in certain cases.
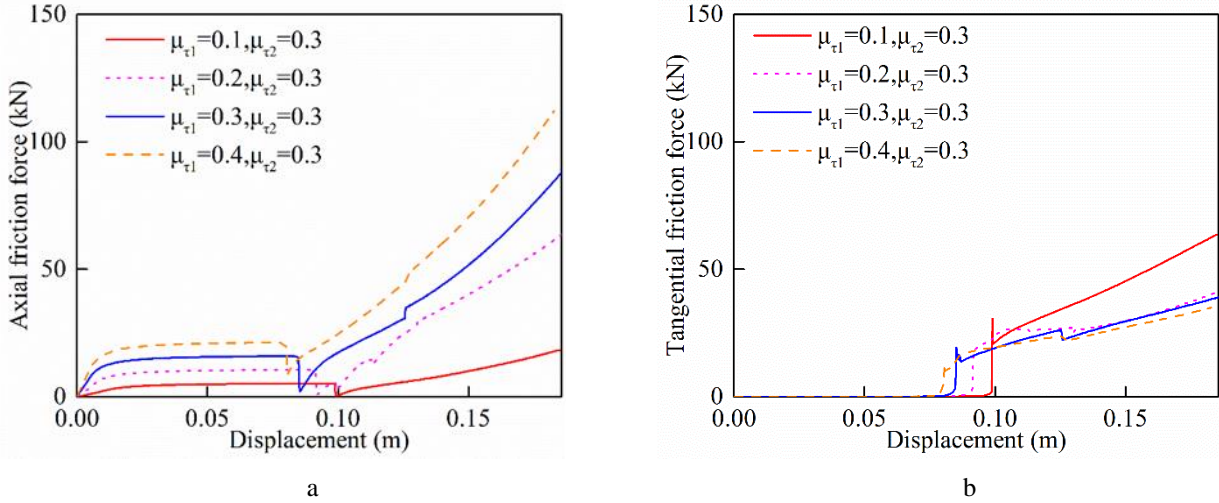

Fig. 6 Effect of axial friction on each frictional force (Case 1): a - axial friction force; b - tangential friction force
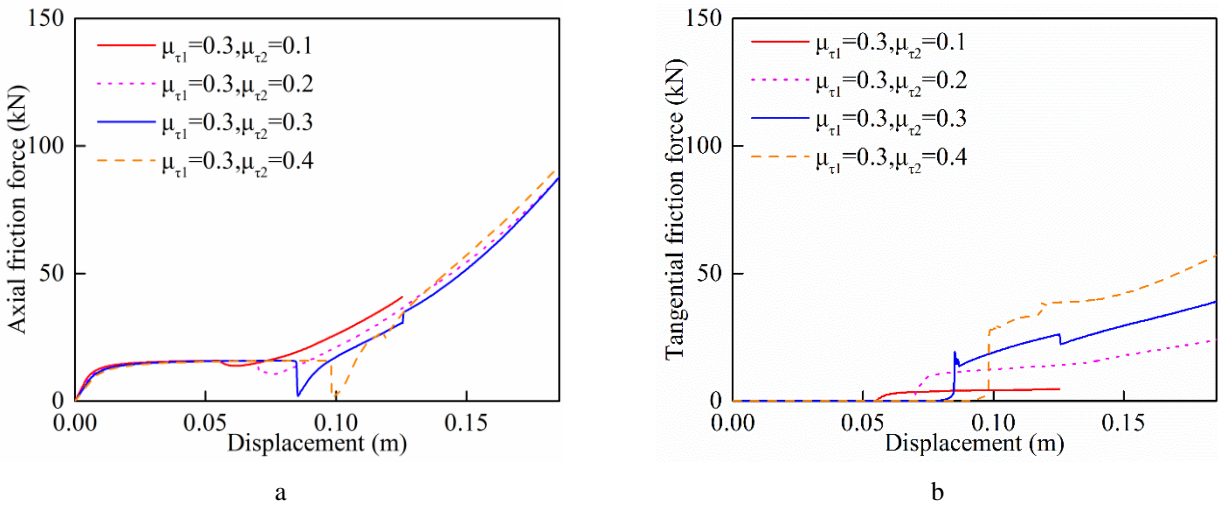

Fig. 7 Effect of tangential friction on each frictional force (Case 2): a - axial friction force; b - tangential friction force
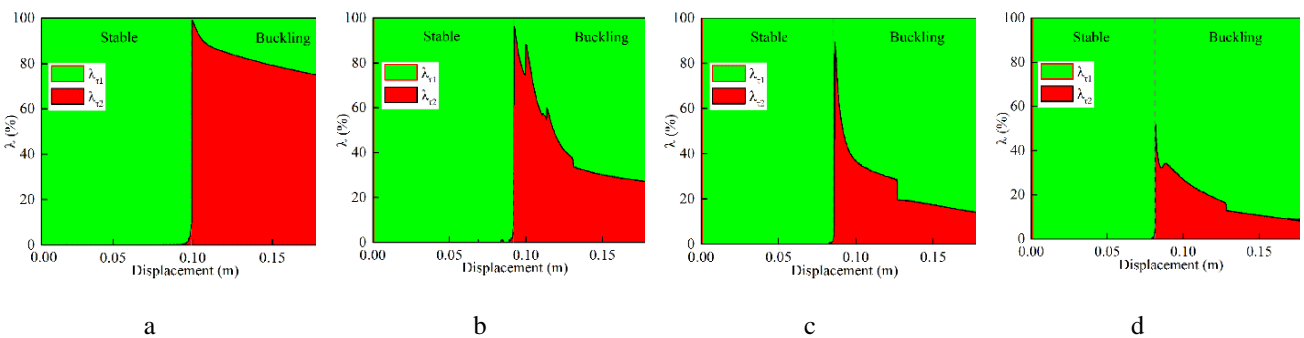

Fig. 8 Effect of axial friction on each frictional force ratio (Case 1): a - $\mu_{\tau 1}=0.1$; b - $\mu_{\tau 1}=0.2$; c - $\mu_{\tau 1}=0.3$; d - $\mu_{\tau 1}=0.4$
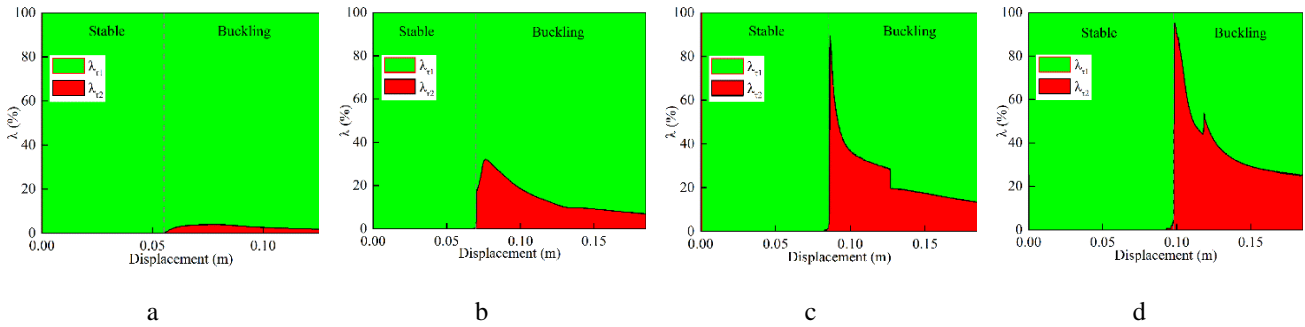
Fig. 9 Effect of tangential friction on each frictional force ratio (Case 2): a - $\mu_{\tau2}$=0.1; b - $\mu_{\tau2}$=0.2; c - $\mu_{\tau2}$=0.3; d - $\mu_{\tau2}$=0.4

3.4. Effect of the orthotropic friction on the axial force transfer

To investigate the effect of the orthotropic friction on the axial force transfer, the axial force transfer efficiency η is defined as the ratio of the bottom force (F_{bottom}) to the top force (F_{top}).

In Fig. 10, we plots the axial force transfer efficiency η as a function of F_{top} in each case. It can be seen that when F_{top} increases, η increases first and then decreases, and reaches the maximum when the sinusoidal buckling is formed. Moreover, the greater the axial friction coefficient, the smaller the axial force transfer efficiency, which dis-

closes the reduction of the axial friction is beneficial to promote the axial force transfer efficiency. The influence of $\mu_{\tau2}$ on the axial force transfer efficiency is mainly in the sinusoidal buckling stage, while the influence in other stages is small.

What discussed in this section suggests that, the axial force transfer is mainly impacted by the axial friction. Compared to the lateral vibration tool (LVT), the axial oscillation tool (AOT) is more suitable to reduce the friction force and improve the axial force transfer efficiency. This conclusion is consistent with the result demonstrated experimentally and numerically by Gee et al. [19].
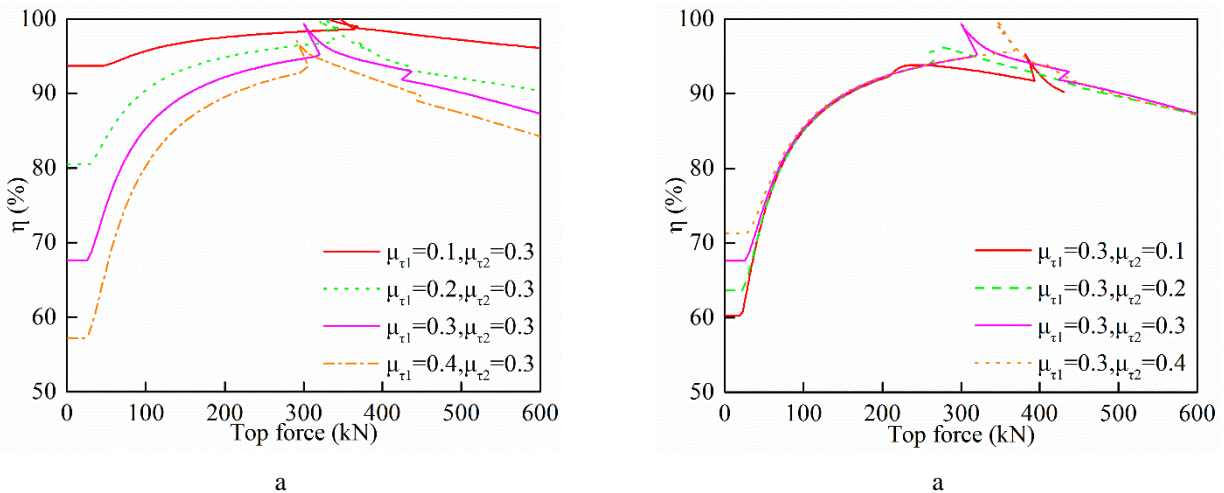

Fig. 10 The effect of the orthotropic friction on the axial force transfer: a – Case 1; b – Case 2

4. Conclusion

In this paper, we establish the buckling model of the horizontal drill string using of finite element method. The influence of the orthotropic friction on the critical buckling force, the bending moment, the friction force and the axial force transfer is systematically analysed. The results show that:

1. The orthotropic friction can impact the critical buckling forces and the buckling configuration. Simplifying the friction between the drill string and the borehole as the unidirectional friction or the isotropic friction cannot accurately predict the buckling behavior.

2. The amplitude of the friction force in each direction and its ratio are all in a variable state. The friction forces may alternately change, and differs with the friction coefficient. The literature hypothesis [6,7] is only valid in certain conditions.

3. The axial force transfer is mainly influenced by the axial friction, and is almost unaffected by the tangential friction. Reducing the axial friction coefficient is more beneficial to improve the axial force transfer.

References

1. **Mitchell, R.F.**1986. Simple Frictional Analysis of Helical Buckling of Tubing. Spe. Drilling Engineering 1(6):457-465.
   https://doi.org/10.2118/13064-PA.

2. **Cunha, J.C.** 2004.Buckling of Tubulars Inside Wellbores: A Review on Recent Theoretical and Experimental Works. Spe Drilling & Completion 19(1):13-19.
https://doi.org/10.2118/87895-PA.

3. **Hajianmaleki, M.; Daily, J. S.** 2014.Advances in critical buckling load assessment for tubulars inside wellbores, Journal of Petroleum Science and Engineering 116 (2):136-144.
https://doi.org/10.1016/j.petrol.2014.02.019.

4. **Gao, D.L.; Huang, W. J**. 2015. A review of down-hole tubular string buckling in well engineering, Petroleum Science 12 (3):443-457.
https://doi.org/10.1007/s12182-015-0031-z.

5. **Gao, D. L.** 2006. Down-Hole Tubular Mechanics and its Application, China University Pettroleum Press Dongying.

6. **Gao, G; Miska, S. Z.**.2009. Effects of boundary conditions and friction on static buckling of pipe in a horizontal well, SPE Journal 14 (4):782-796.
https://doi.org/10.2118/111511-PA.

7. **Gao, G; Miska, S. Z.** 2010. Effects of friction on postbuckling behavior and axial load transfer in a horizontal well, SPE Journal 15 (4):1104-1118.
https://doi.org/10.2118/120084-MS.

8. **Hajianmaleki, M; Daily, J. S**. 2014. Critical-Buckling-Load Assessment of Drillstrings in Different Wellbores by use of the Explicit Finite-Element Method, Spe Drilling & Completion 29 (2):256-264.
https://doi.org/10.2118/166592-PA.

9. **Miller, J. T; Su, T.; Pabon, J; Wicks, N.; Bertoldi, K.; Reis, P. M**. 2015. Buckling of a thin elastic rod inside a horizontal cylindrical constraint, Extreme Mechanics Letters 3:36-44.
https://doi.org/10.1016/j.eml.2015.03.002.

10. **Gaynor, T. M.; Chen, D. C.-K.; Stuart, D.; Comeaux, B.** 2001.Tortuosity versus Micro-Tortuosity-Why Little Things Mean a Lot, in: SPE/IADC Drilling Conference, https://doi.org/10.2118/67818-MS.

11. **Samuel, G.R.; Bharucha, K., Luo, Y**. 2005.Tortuosity Factors for Highly Tortuous Wells: A Practical Approach. in: SPE/IADC Drilling Conference.
https://doi.org/10.2118/92565-MS.

12. **Marck, J; Detournay, E.** 2015. Spiraled Boreholes: An Expression of 3D Directional Instability of Drilling Systems. SPE Journal 21(2): 434-448.
https://doi.org/10.2118/173156-PA.

13. **Marck, J.; Detournay, E.** 2016. Influence of Rotary-Steerable-System Design on Borehole Spiraling, SPE Journal 21(1): 293-302.
https://doi.org/10.2118/174554-PA.

14. **Olofsson, U; Hagman, L.** 1997. A model for micro-slip between flat surfaces based on deformation of ellipsoidal elastic bodies, Tribology International 30(8):599-603.

https://doi.org/10.1016/S0301-679X(97)00028-5.

15. **Wang, P.; Ni, H.; Wang, R.; Li, Z.; Wang, Y.** 2016. Experimental investigation of the effect of in-plane vibrations on friction for different materials, Tribology International 99:237-247.
https://doi.org/10.1016/j.triboint.2016.03.021.

16. **Dykstra Mark, W.** 1996. Nonlinear Drill String Dynamics. Ph D Dissertation, University of Tulsa.

17. **Lian, Z.; Zhang, Q; Lin, T.; Wang, F.** 2015. Experimental and numerical study of drill string dynamics in gas drilling of horizontal wells, Journal of Natural Gas Science and Engineering 27(3):1412–20.
https://doi.org/10.1016/j.jngse.2015.10.005.

18. **Gee, R.; Hanley, C.; Hussain, R.; Canuel, L.; Martinez, J.** 2015. Axial Oscillation Tools vs. Lateral Vibration Tools for Friction Reduction – What's the Best Way to Shake the Pipe?, in: SPE/IADC Drilling Conference and Exhibition.
https://doi.org/10.2118/173024-MS.

Jianxun Liu, Hualin Zheng, Yuchun Kuang, Xiaofeng Xu, Yonghui Liu

NUMERICAL SIMULATION OF THE DRILL STRING BUCKLING BEHAVIOR IN HORIZONTAL WELLS CONSIDERING THE ORTHOTROPIC FRICTION

S u m m a r y

The effect of the friction between the drill string and the borehole on the drill string buckling behavior has not been fully understood. First, we treated the friction between the drill string and the borehole as the orthotropic friction, and established a finite element (FE) model of the drill string and the borehole system. Then, the comparison with the experimental results shows that the FE model has a high accuracy. Finally, the effect of the orthotropic friction on the buckling behavior of the drill string was analyzed. Results demonstrate that the orthotropic friction can impact the buckling behavior, such as the critical buckling forces, the bending moment, the friction force and the axial force transfer. Simplifying the friction between the drill string and the borehole as the unidirectional or the isotropic friction cannot accurately predict the buckling behavior. The results can complement the existing theoretical models and provide guidance for field operations.